Electronic Supplementary Material (ESI) for Energy Advances.

Supporting Information

Promoting water splitting reaction on TiO_2/gCN with Pd/SrO cocatalysts: H_2 evolution in absence of sacrificial reagent†

Khezina Rafiq[a], Kashaf Ul Sahar[a], Muhammad Zeeshan Abid[a], Saira Attique[a], Ubaid ur Rehman[b], Abdul Rauf[a], Ejaz Hussain[a*]

[a]Institute of Chemistry, Inorganic Materials Laboratory 52S, The Islamia University of Bahawalpur-63100, Pakistan

[b]School of Physics, State Key Laboratory of Crystal Materials, Shandong University, Jinan 250100, Shandong, China

Corresponding authors: Dr. Ejaz Hussain; ejaz.hussain@iub.edu.pk

Dr. Khezina Rafiq; khezina.rafiq@iub.eu.pk

Section 1

1.1. Experimental

1.1.1. Chemicals required

The analytical grade chemicals that were utilized in this study were procured from commercial sources and were not subjected to further modifications. Melamine (CAS 108-78-1) and rutile TiO2 (CAS 1317-80-2) were brought from Hqauiang Chemical Group Stock Co., LTD and Texan Minerals & Chemicals. The salt of palladium (II) acetate was purchased from CATO Research Chemicals Inc, and strontium chloride hexahydrate 99% (Sigma-Aldrich, CAS Number 10025-70-4). The highly purified deionized H_2O was aided by PIAS Pakistan (PIAS-GW1-Z).

1.1.2. Synthesis of gCN

To prepare gCN, melamine (5 g) was placed in alumina-cylindrical crucible with a lid and heated in the muffle furnace at 350 ^{0}C for nine hours. The furnace was heated at the rate of 5 ^{0}C/min and the yellowish powder was obtained. This synthetic method involves calcination and ensures the purity of final product.

1.1.3. Synthesis of TiO_2/gCN

In a three neck round bottom flask, 200 mg of gCN was dispersed in 50 mL of DI-H_2O and stirred for 2h at room temperature. Following the 10 minutes of sonication, 200 mg of TiO_2 was added and stirred again for 30 minutes. Then, the slurry was sonicated for 10 minutes and again placed on magnetic stirrer for 30 minutes of stirring. The slurry was transferred to Teflon-Lined-Autoclave and placed in the oven for 2h at 150 ^{0}C for hydrothermal reaction. The slurry was removed from autoclave and underwent filtered. Following this, the resultant sample was left to

dry overnight (80 ^{0}C) in order to obtain solid matter. Subsequently, the solid was grounded to the fine particles and placed in the crucible fitted with the lid, before being position in the muffle furnace. The final product was ultimately obtained after undergoing calcination for the period of 5h.

1.1.4. Synthesis of Pd@TiO_2/gCN

During the process of synthesizing TiO_2/gCN, which was explained in TiO_2/gCN synthesis, a 2 % ml solution of palladium (II) acetate was added to TiO_2/gCN mixture before it underwent a hydrothermal treatment. The mixture was stirred for 30 minutes and then sonicated for 10 minutes. After this 30 mg of $NaBH_4$ dissolved in 20 mL of water and added that solution into the prepared slurry. The milky slurry underwent a transformation, turning from white to grey with the emergence of bubbles. After being sonicated for 10 minutes, it was placed in an autoclave to undergo a hydrothermal treatment. The resulting product was filtered, dried and finally calcined.

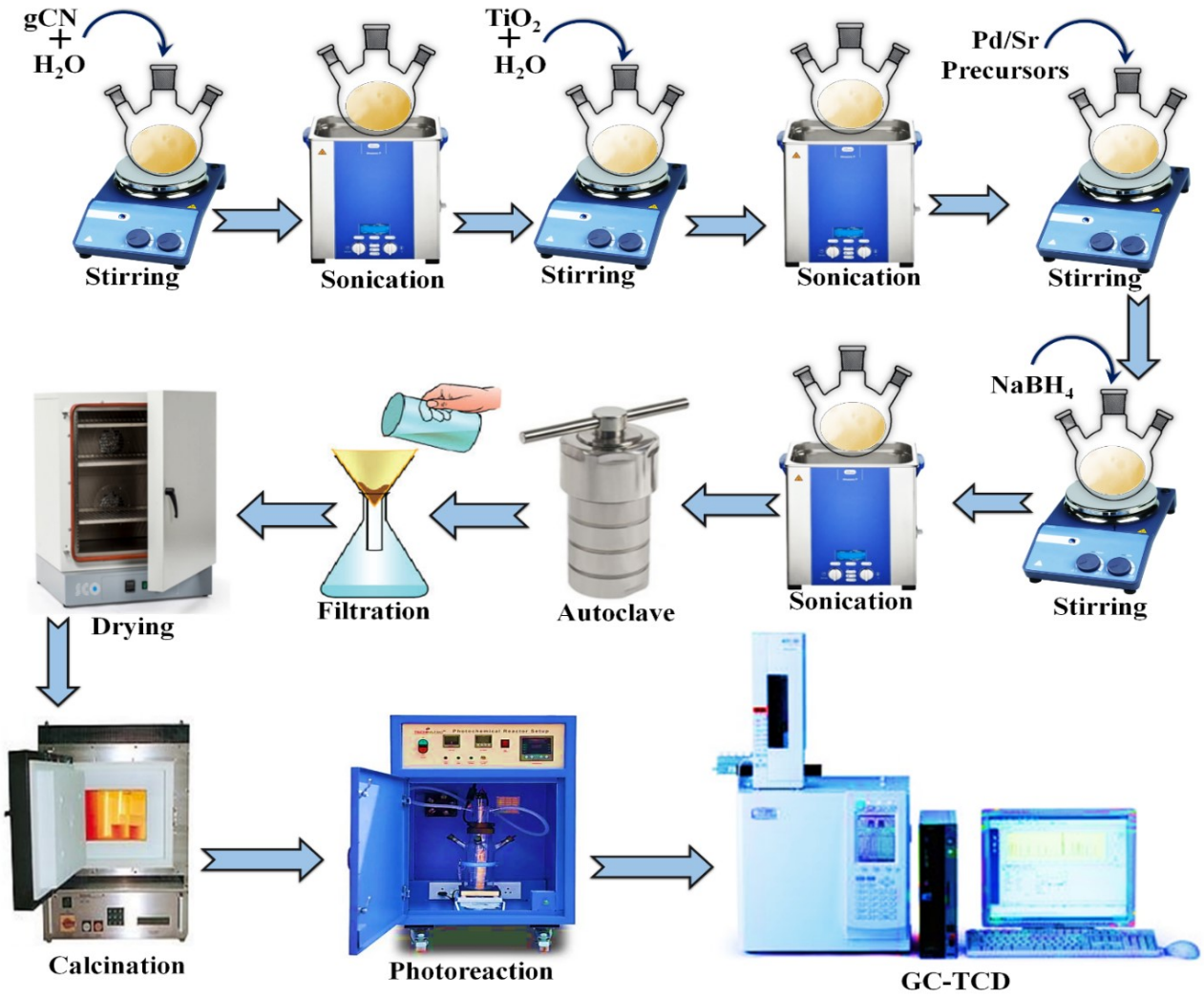

Figure.S1 The scheme of Pd-SrO@TiO_2/gCNphotocatalysts synthesis

1.2. Instruments used for characterization

Powder X-Ray diffraction patterns were measured X-ray diffractometer with Ni filtered utilizing Cu-Kα radiations as X-ray source whose wavelength was approximately1.5418Å while the X-ray beam intensity was set to 40 mA as well as the X-ray tube voltage was set to 40kV. Data was composed by operating flat-plate holder in Bragg−Brentano Parafocusing Geometry, it helped to identify a crystallinity of synthesized material.Fourier Transform Infrared spectra was attained by utilizing potassium bromide matrix tablet in Nicolet Avatar 330 FTIR spectrometer with the

unit of cm^{-1} which helped to specify the position of absorption bands, functional groups and chemical bonds. The surface morphology and composition of the synthesized materials were identified by SEM analysis via Thermo Fisher AxiaChemiSEM. The UV-DRS spectra was obtained via UV-Vis spectrophotometer by Thermo Fischer scientific and moulded with the Praying Mantis Diffuse Reflectance Adapter. Foe chemical composition and surface analysis, XPS spectra of as synthesized catalysts were obtained byKratos Axis UlraDLDfixed with Hemispherical Deflection Analyzer and chamber to separate the electrons and measure different kinetic energies emitted from the sample. The monochromatic Al Kα rays with photon energy of 1486.6–69 eV, produced by an X-rays that produces 150 W of power. For examination, samples were cautiously pressed into the small pellets with the width of 0.1 mm. The Horiba JY LabRAM HR 800 (high resolution Raman spectrometer) equipped with microscopeutilized to study the vibrational, rotational and low frequency modes of molecules in the synthesized material. He-Ne laser with the wavelength of 632.8 nm was utilized as excitation source while the laser was operated at 20 mV. The spectral resolution of Raman Spectrometer was set to 0.35 cm^{-1} while D4 filter was used to augment the features of gCN, in spectral range of $1300 - 1800$ cm^{-1}. To analyze the optical and electronic properties, Photoluminescence Spectroscopy was performed by utilizing Custom Cryogenic Macro PL System (CCMPS) fixed with HORIBA components (325 nm laser). The iHR320 was an imaging spectrometer used to disperse and measured the wavelength of emitted and scattered light while the detection was made by Syncerity Charged-Coupled device. AFM done through PARK N×10 instrument that was used to govern the mechanical properties and localization of the loaded metals over the surfaces of photocatalysts.The specified surface are and the diameters of the pores seizes, pore size distribution and specific surface area were analyzed by BrunauerEmmmet

Teller (BET) technique. The electrochemical workstation (CHI660E Instruments) has been utilized to analyze the photoelectrochemical properties of synthesized photocatalysts by electrochemical impedance spectroscopy (EIS).

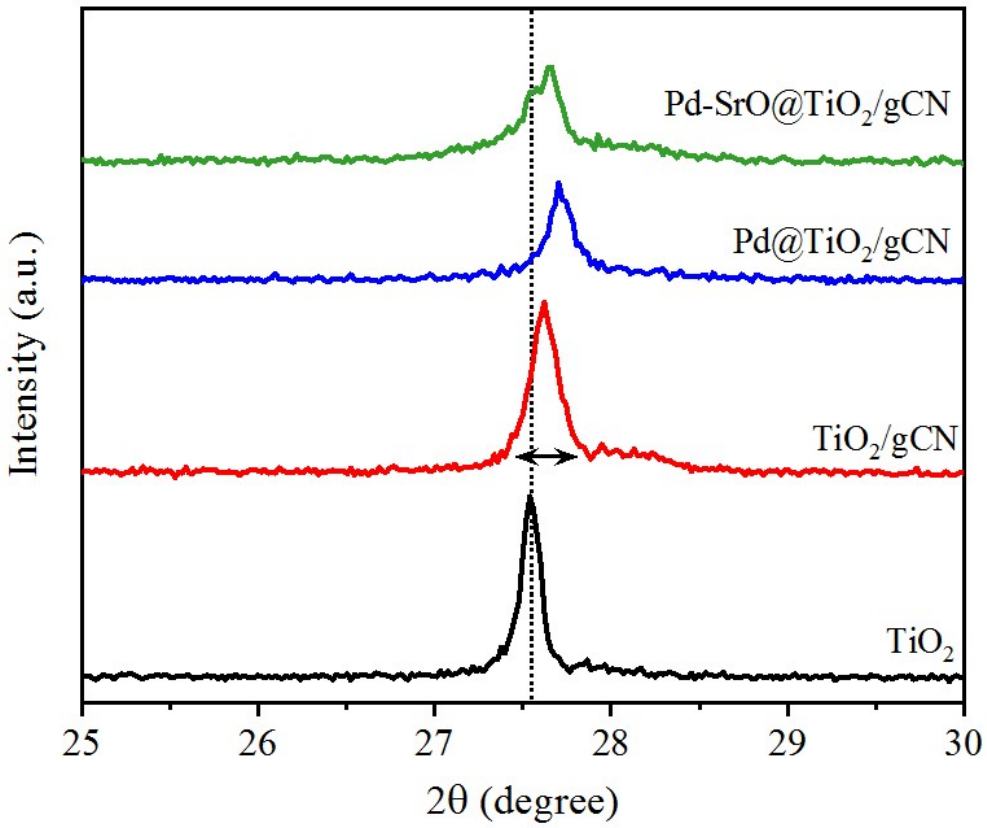

Figure.S2 XRD pattern of TiO_2, TiO_2/gCN, Pd@TiO_2/gCN, and Pd-SrO@TiO_2/gCN in the range of 25–30°.

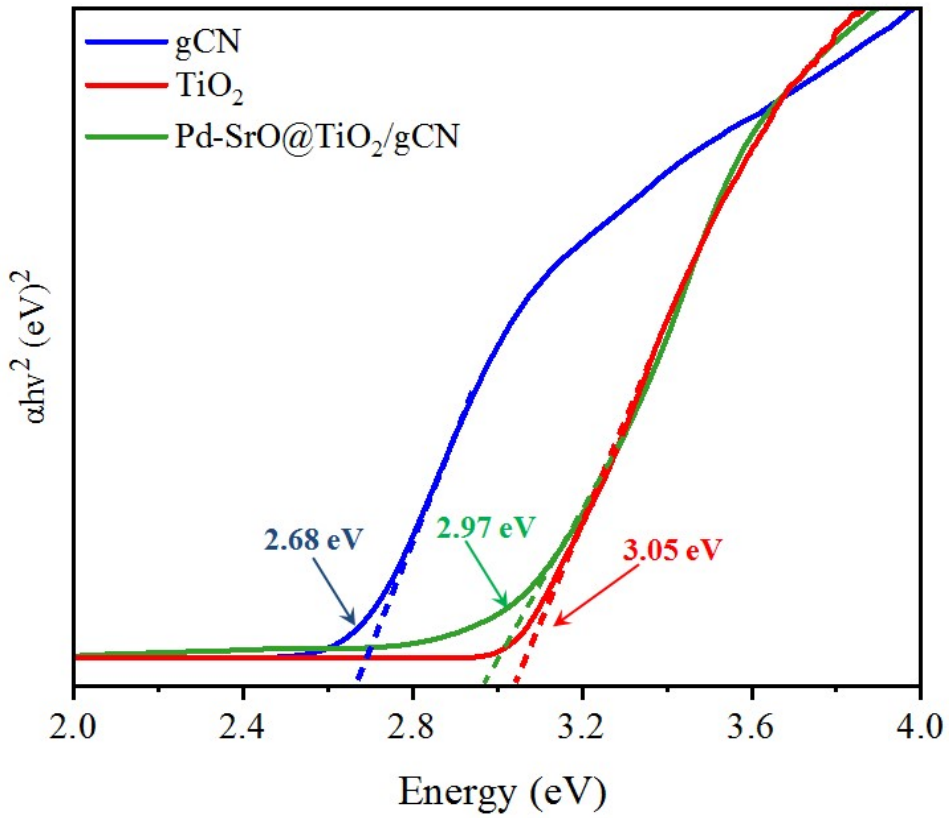

Figure.S3 Tauc plot of gCN, TiO_2 and Pd-SrO@TiO_2/gCN catalysts in the range of 2.0–4.0 eV

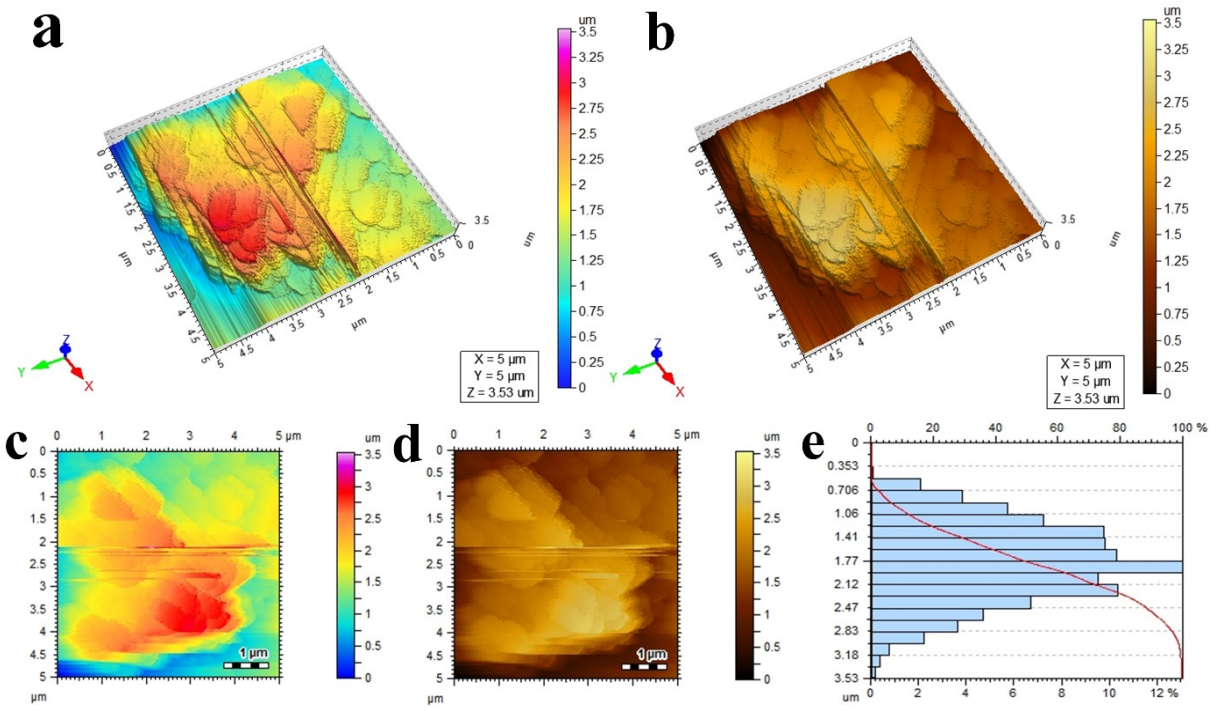

Figure S4. AFM topography of Pd-SrO@TiO_2/gCN (a) 3D image in light irradiation (b) 3D image in dark (c) 2D image in light (d) 2D image in dark (e) Height portfolio of particles.

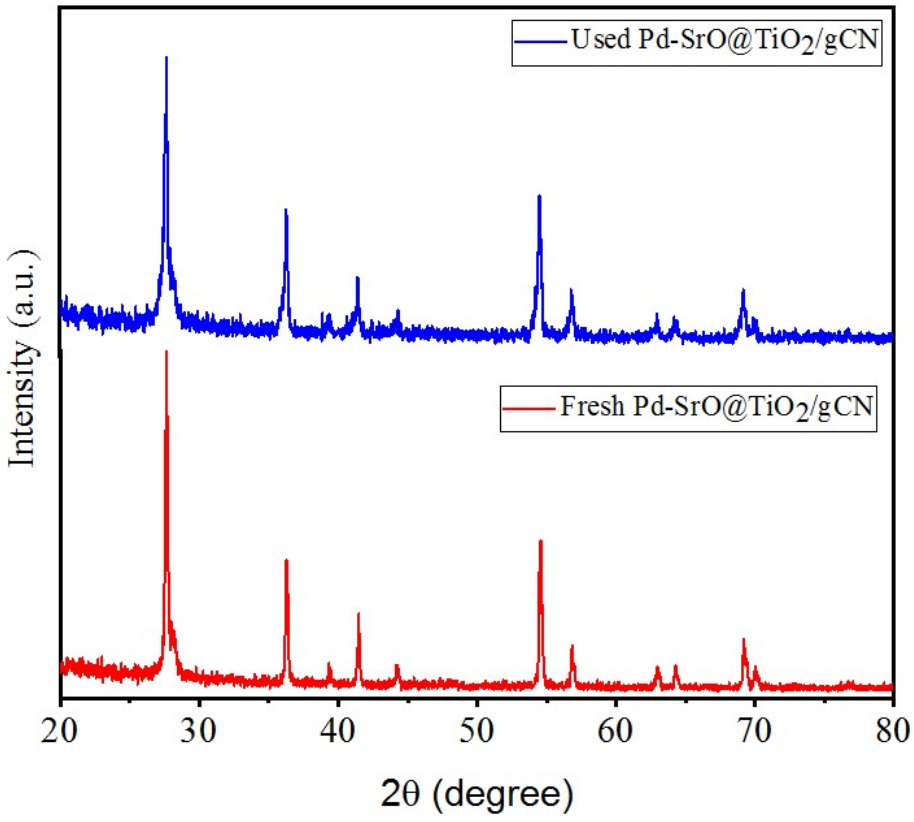

Figure.S5 XRD results of used and fresh Pd-SrO@TiO_2/gCN catalysts.

1.3. Recyclability test:

Table S1. Recyclability test for the most active photocatalysts (Pd-SrO@TiO_2/gCN)

Photocatalysts (Pd-SrO@TiO_2/gCN)	**Time (h)**						**H_2 generation**
	1	2	3	4	5	6	
1st run	24.5	49.0	73.5	98.0	122.5	147.0	mmol g^{-1}
2nd run	22.5	44.0	66.5	89.0	111.5	134.0	mmol g^{-1}
3rd run	20.5	41.0	61.5	82.0	102.5	123.0	mmol g^{-1}

Section 2

2.1. Factors impact on the H_2 production capacity by photocatalysts

2.1.1. Effect of light intensity

Hydrogen evolution activities were conducted in natural sunlight.The hydrogen evolution directly influenced by upon the intensity of light[1, 2]. In current study, the photoreaction was conducted for 6 hours under solar irradiations in October 2023, at the Islamia University of Bahawalpur, Pakistan. The highest recorded rate of H_2 evolution was 24.5 $mmolg^{-1}$ h^{-1} during the fourth hour of photoreaction between 1:00 PM and 2:00 PM. The surface of photocatalysts experienced highest level UV exposure (520 Wm^{-2})[3]. Less rate of hydrogen evolution observed in other time durations is depicted in Figure.7a (main manuscript) and Table. S2. The reason is that the earth is most exposed to sunlight around solar noon, which is in the middle of the day, as this is when the sun reaches its highest point in the sky, resulted in the maximum amount of solar energy provided to the reaction system[4].

Table S2. Influence of light intensity onH_2 evolution byPd-SrO@TiO_2/gCNin different time-frames by using most active photocatalysts

Serial No	Photocatalysts	Time (6h) under Sun-light	H_2 Evolution (mmol $g^{-1}h^{-1}$)
1	Pd-SrO@TiO_2/gCN	10:00 AM-11.00 AM	10.3
2	Pd-SrO@TiO_2/gCN	11:00 AM-12:00 PM	15.4
3	Pd-SrO@TiO_2/gCN	12:00 PM-1:00 PM	19.7
4	Pd-SrO@TiO_2/gCN	1:00 PM-2:00 PM	24.5
5	Pd-SrO@TiO_2/gCN	2:00 PM-3:00 PM	20.3
6	Pd-SrO@TiO_2/gCN	3:00 PM-4:00 PM	18.2

2.1.2. Effect of pH

In neutral or slightly basic medium, the rate of H_2 evolution can be quite high due to presence of enough protons (H^+) for their reduction to form hydrogen gas, which eventually lead to the favourable equilibrium between the two-half reactions in water splitting. We conducted an experiments on the impact of different pH (levels) in order determine the optimal for hydrogen production, utilizing hydrochloric acid and sodium hydroxide for pH optimization. Pd-SrO@TiO_2/gCN delivered maximum hydrogen production at the rate of 24.5mmol $g^{-1}h^{-1}$ at pH 7.5. The reason is that, under the conditions of pH neutrality, there was a moderate concentration of protons and hydroxide ions, creating an environment conducive to facilitate water splitting reaction and ultimately gave efficient H_2 gas evolution. While neutral pH conditions are less corrosive to photocatalysts and better for maintaining its stability. The H_2 production activities over all as synthesised photocatalysts at different pH have been evaluated as illustrated in Table S3 and Figure. 7d (main manuscript).

In acidic medium, the concentration of protons is relatively low due to the presence of H_3O^+ ions in water, which decrease the rate of reduction reaction and leads to slower hydrogen production. That's why the rate of hydrogen production has been decreased below pH 7.5.

$$2H_2O_{(l)} \rightarrow 2H_{2\,(g)} + O_{2\,(g)}$$

$$2H^+_{(aq)} + 2e^- \rightarrow H_{2\,(g)}$$

Similarly, in case of highly alkaline medium, the corrosion of material chances has been increased to maximum level as well as the concentration of hydroxide ion is very high and availability of proton for reduction of H+ ions is very low (above pH 7.5). Thus, the rate of hydrogen production has been also decreased in highly alkaline medium[5, 6].

$$2H_2O + 2e^- \rightarrow H_{2\,(g)} + 2OH^-_{(aq)}$$

Table S3. Influence of pH onH_2 evolution by using most active photocatalysts Pd-SrO@TiO_2/gCN

Serial No	Photocatalysts	pH	H_2 Evolution (mmol $g^{-1}h^{-1}$)
1	Pd-SrO@TiO_2/gCN	4.0	3.2
2	Pd-SrO@TiO_2/gCN	4.5	6.2
3	Pd-SrO@TiO_2/gCN	5	9.1
4	Pd-SrO@TiO_2/gCN	5.5	12.9
5	Pd-SrO@TiO_2/gCN	6	15.3
6	Pd-SrO@TiO_2/gCN	6.5	18.5
7	Pd-SrO@TiO_2/gCN	7	21.4
8	Pd-SrO@TiO_2/gCN	7.5	24.5
9	Pd-SrO@TiO_2/gCN	8	19.1
10	Pd-SrO@TiO_2/gCN	8.5	16.9

2.1.3. Effect of sacrificial reagent

We have investigated different sacrificial reagents (EDTA [7], Glycerol [8], Lactic acid, Methanol, Ethanol , and TEOA) to evaluate their effects H_2 evolution by Pd-SrO@TiO_2/gCN[9,

10]. Less rate of hydrogen evolution has been observed in presence of all different sacrificial reagents as compared to utilizing metal oxide (SrO) with Pd@TiO_2/gCN, as represented in, Table S4 and Figure.7c. The reason is that When the sacrificial reagents are used, it brings the more chemical reaction and by products. Introducing the sacrificial reagents into the reaction has increased its complexity, since multiple reactions take place simultaneously. The use of organic sacrificial reagents possess leads to constant replenishment and increased operational cost. The objectionable roles of sacrificial reagents are, the catalysts poisoning, as well as toxic intermediates and by-products origination during reactions that could accumulate and have potential impact on the performance of photocatalysts in the long run and ultimately decrease the rate of hydrogen evolution[11-13].

In the current study, the maximum hydrogen produced over Pd-SrO@TiO_2/gCN (24.5 mmol $g^{-1}h^{-1}$), when no additional sacrificial was utilized for the purpose of holes consumption. Strontium oxide augmented the consumption of holes from the valance band. The SrO interacted with H_2O and resulted in the splitting it into H^+ and OH^- ions. The OH^- ions quickly reacted with holes and drained their presence in the photocatalytic system. Subsequently the recombination of charge carriers was significantly lessened. Hence, the maximum reduction in activation energy threshold separating oxidation from reduction potential was achieved upon the introduction of dual co-catalysts (strontium oxide and palladium) on to the semiconductor surfaces.

Table S4. Influence of sacrificial reagent on H_2 evolution on as synthesised photocatalysts

Serial No	Photocatalysts	Sacrificial reagent	H_2 Evolution (mmol $g^{-1}h^{-1}$)
1	Pd@TiO_2/gCN	EDTA	10.4
2	Pd@TiO_2/gCN	Glycerol	11.6
3	Pd@TiO_2/gCN	Lactic acid	15.7
4	Pd@TiO_2/gCN	Methanol	18.4
5	Pd@TiO_2/gCN	Ethanol	21.1
6	Pd@TiO_2/gCN	TEOA	22.3
7	Pd-SrO@TiO_2/gCN	-	24.51

2.1.4. Effect of dose

The effect of dose concentration of catalysts on hydrogen evolution through the reaction of water splitting was investigated. In recent research, the optimal concentration of photocatalysts (Pd-SrO@TiO_2/gCN) that generated 24.5 mmol $g^{-1}h^{-1}$ of hydrogen was determined to be 5 mg.The increase in a dose concentration of photocatalysts resulted in decreasing rate of hydrogen evolution because of agglomeration of nanoparticles, increase in optical density of solution in the reactor, mass transport limitation, increase in recombination of electrons, and light absorption competition in each particle. Above 5 mg dose concentration, the rate of hydrogen production has been decreased[14], as represented in Table S5 and Figure. 7b.

Table S5. Effect of photocatalysts dose on hydrogen evolution (mmol $g^{-1}h^{-1}$) over Pd/Au@g-C_3N_4/TiO_2

Serial No	Photocatalysts	Concentration	Hydrogen evolution (mmol $g^{-1}h^{-1}$)
1	Pd-SrO@TiO_2/gCN	1 mg	8.5
2	Pd-SrO@TiO_2/gCN	2 mg	13.8
3	Pd-SrO@TiO_2/gCN	3 mg	15.7
4	Pd-SrO@TiO_2/gCN	4 mg	20.4
5	Pd-SrO@TiO_2/gCN	5 mg	24.5
6	Pd-SrO@TiO_2/gCN	6 mg	21.1
7	Pd-SrO@TiO_2/gCN	7 mg	17.9
8	Pd-SrO@TiO_2/gCN	8 mg	15.1

2.1.5. Effect of weight % loading of metal and metal oxide:

In general, our objective was to achieve a harmonious equilibrium between the presences of sufficient metal oxide loading over semiconductor surfaces to aid in the charge separation and catalysis, all the while the circumventing the drawbacks that come with the heavy loading such as diminished light adsorption and limitation in mass transport. In recent research we have performed different reactions by varying the amount percentage loading of strontium oxide to maintain overall 2 w % loading of cocatalysts (Pd:SrO) over semiconductor[15]. Maximum

hydrogen production (24.5 mmol $g^{-1}h^{-1}$) has been observed over Pd-SrO@TiO_2/gCN when the Pd: SrO was 1.8:0.2. The increase in the concentration of palladium increases the rate of hydrogen production, while increase in the w % loading of strontium caused decrease in rate of hydrogen production as represented in Table S6 and Figure. 7e. It has been observed that increasing the recommended amount of metal oxide loading resulted in problem with stability and compatibility, including added stress over photocatalysts that may an impact on its durability and effectiveness.

Table S6. Hydrogen generation rate at distinct amounts (Vol %) of sacrificial reagent

Prepared photocatalysts	**Weight % loading of metal and metal oxide**		**H_2 Evolution (mmol $g^{-1}h^{-1}$)**
Pd-SrO@TiO_2/gCN	Palladium	Strontium oxide	
Pd-SrO@TiO_2/gCN	0.2	1.8	9.4
Pd-SrO@TiO_2/gCN	0.4	1.6	11.1
Pd-SrO@TiO_2/gCN	0.6	1.4	13.9
Pd-SrO@TiO_2/gCN	0.8	1.2	15.8
Pd-SrO@TiO_2/gCN	1	1	16.7
Pd-SrO@TiO_2/gCN	1.2	0.8	18.9
Pd-SrO@TiO_2/gCN	1.4	0.6	20.3
Pd-SrO@TiO_2/gCN	1.6	0.4	22.1
Pd-SrO@TiO_2/gCN	1.8	0.2	24.5

2.1.6. Effect of temperature:

In current research work, 60 ^{0}C was found to be an optimized temperature and 24.5 mmol $g^{-1}h^{-1}$ of hydrogen evolved. The reactions have been performed in the temperature ranges from 20^{0}C to 90 ^{0}C. The rate of H_2 evolution is considerably affected by temperature.The factors like enhanced thermal activity, fast reaction kinetics, enhanced ion mobility, improved catalysts activity, and increased solubility of gases have been observed with the increase in temperature during hydrogen production reaction. But when the temperature started to increase above 60 ^{0}C the rate of hydrogen production has been decreased because of corrosion and degradation of photocatalysts at high temperature[16] as represented in Figure. 7f and Table S5.

Table S7. Influence of temperature on hydrogen evolution (mmol $g^{-1}h^{-1}$) over Pd-SrO@TiO_2/gCN

Serial No	Photocatalysts	Temperature ˚C	Hydrogen evolution (mmol $g^{-1}h^{-1}$)
1	Pd-SrO@TiO_2/gCN	20	10.5
2	Pd-SrO@TiO_2/gCN	30	14.3
3	Pd-SrO@TiO_2/gCN	40	17.6
4	Pd-SrO@TiO_2/gCN	50	21.3
5	Pd-SrO@TiO_2/gCN	60	24.5
6	Pd-SrO@TiO_2/gCN	70	20.1
7	Pd-SrO@TiO_2/gCN	80	17.3
8	Pd-SrO@TiO_2/gCN	90	12.5

Section 3

Table S8. Assessmentof Q.E.Y of as-synthesized photocatalysts (Pd-SrO@TiO_2/gCN) with other gCN heterojunctions based semiconductors reported in the literature (in year 2023 & 2024).

Photocatalyst	**Synthesis Technique**	**Sacrificial reagent**	**H_2 production (mmol g^{-1} h^{-1})**	**A.Q.E %**	**Ref.**
Pd-SrO@TiO_2/gCN	Hydrothermal	Absent	24.5	18.5	-
Mo@2D/2D g-C_3N_4/MoS_2	Exfoliation	TEOA	2.2226	9.08	[17]
Cu_2MoS_4/g-C_3N_4	Oil bath method	TEOA	2.385	-	[18]
CdSe QDs/g-C_3N_4	Ionic layer adsorb/SILAR	TEOA	23.8	4.306	[19]
Pt-N@g-C_3N_4	Impregnation method	TEOA	0.3368	13.5	[20]
Bi_2O_2Se/g-C_3N_4	Thermal/Liquid exfoliation	-	6.481	11.65	[21]
UiO-66@g-C_3N_4/Ni	Solvothermal approach	TEOA	2.6	6.41	[22]
EP-Dy_2O_3/g-C_3N_4	High temperature pyrolysis	Glucose	0.723	-	[23]
g-C_3N_4/CdS@C	Hot Polymerization	Ethanol	6.4	12.7	[24]
VPQDs/g-C_3N_4	Electronic pulse excitation	TEOA	7.7	11.68	[25]
Ni–$CuWO_4$/g-C_3N_4	Chemical precipitation	Ethanol	1.98	6.49	[26]
g-C_3N_4@Ca/UiO-66	Solvothermal approach	SO_3^{2-}, S^{2-}	0.1783	13.85	[27]
HOFs/CNNS	In situ electrostatic interaction	Ethanol	4.45	22	[28]
$NiCo_2S_4$/C_3N_4-*x*	Hydrothermal	TEOA	15.673	-	[29]
g-C_3N_4/$Ti_3C_2T_x$	Calcination/HF etching	Methanol	1.912	3.1	[30]

S.R= Sacrificial Reagent, A.Q.E= Apparent Quantum Yield, adsorp*= Adsorption

Reference

1. Nishioka, S., et al., Excited carrier dynamics in a dye-sensitized niobate nanosheet photocatalyst for visible-light hydrogen evolution. ACS Catalysis, 2020. **11**(2): p. 659-669.
2. Chen, D., et al., Nanospherical like reduced graphene oxide decorated TiO2 nanoparticles: an advanced catalyst for the hydrogen evolution reaction. Scientific reports, 2016. **6**(1): p. 20335.
3. Sahar, K.U., et al., Surface sensitization of g-C3N4/TiO2 via Pd/Rb2O cocatalysts: Accelerating water splitting reaction for green fuel production in the absence of organic sacrificial agents. Reaction Chemistry & Engineering, 2023.
4. Resendiz, E.M., et al., Analysis of a small-scale modified beam-down solar concentrator system for low temperature applications. Renewable Energy, 2023. **215**: p. 119007.
5. Tiwari, A., I. Mondal, and U. Pal, Visible light induced hydrogen production over thiophenothiazine-based dye sensitized TiO 2 photocatalyst in neutral water. Rsc Advances, 2015. **5**(40): p. 31415-31421.
6. Dinda, D., et al., Amorphous molybdenum sulfide quantum dots: an efficient hydrogen evolution electrocatalyst in neutral medium. Journal of Materials Chemistry A, 2016. **4**(40): p. 15486-15493.
7. Galińska, A. and J. Walendziewski, Photocatalytic water splitting over Pt− TiO2 in the presence of sacrificial reagents. Energy & Fuels, 2005. **19**(3): p. 1143-1147.
8. Tahir, M., La-modified TiO2/carbon nanotubes assembly nanocomposite for efficient photocatalytic hydrogen evolution from glycerol-water mixture. International Journal of Hydrogen Energy, 2019. **44**(7): p. 3711-3725.
9. Bajpai, H., et al., Biomass components toward H 2 and value-added products by sunlight-driven photocatalysis with electronically integrated Au δ−–TiO 2: concurrent utilization of electrons and holes. 2023.
10. Sabir, A.S., et al., An inclusive review and perspective on Cu-based materials for electrochemical water splitting. 2023. **13**(8): p. 4963-4993.
11. Sahar, K.U., et al., Surface sensitization of gC 3 N 4/TiO 2 via Pd/Rb 2 O co-catalysts: accelerating water splitting reaction for green fuel production in the absence of organic sacrificial agents. Reaction Chemistry & Engineering, 2023.
12. Nishioka, S., et al., Photocatalytic water splitting. Nature Reviews Methods Primers, 2023. **3**(1): p. 42.
13. Schneider, J. and D.W. Bahnemann, Undesired role of sacrificial reagents in photocatalysis. 2013, ACS Publications. p. 3479-3483.
14. Saleem, F., et al., Synergistic effect of Cu/Ni cocatalysts on CdS for sun-light driven hydrogen generation from water splitting. International Journal of Hydrogen Energy, 2023.
15. Sahar, K.U., et al., Sun-light driven hydrogen generation by Pd/Rb2O cocatalysts: Escalate the utility of rutile TiO2 for photocatalytic water splitting. Colloids and Surfaces A: Physicochemical and Engineering Aspects, 2023. **674**: p. 131942.
16. Zhang, G., et al., Metal sulfides for photocatalytic hydrogen production: Current development and future challenges. Solar Rrl, 2022. **6**(10): p. 2200587.
17. Wang, H., et al., Integrating configuration, doping and heterojunction into the g-C3N4-based photocatalyst for water splitting. Carbon, 2024. **218**: p. 118723.

18. Sun, Y., et al., Ultrathin Cu2MoS4/g-C3N4 nanosheets for promoting charge separation with strong redox ability and enhanced photocatalytic hydrogen production activity. Colloids and Surfaces A: Physicochemical and Engineering Aspects, 2024. **684**: p. 133156.
19. Mehtab, A. and T. Ahmad, Unveiling the bifunctional photo/electrocatalytic activity of in situ grown CdSe QDs on g-C3N4 nanosheet Z-scheme heterostructures for efficient hydrogen generation. ACS Catalysis, 2024. **14**(2): p. 691-702.
20. Zhang, Q., et al., Accelerating photocatalytic hydrogen production by anchoring Pt single atoms on few-layer g-C3N4 nanosheets with Pt-N coordination. Journal of Materials Chemistry C, 2024.
21. Lin, C., et al., Improving photocatalytic hydrogen generation of g-C3N4 via efficient charge separation imposed by Bi2O2Se nanosheets. Carbon, 2024. **218**: p. 118721.
22. Jamma, A., et al., Defect-rich UiO-66@ gC 3 N 4/Ni frameworks as efficient water splitting photocatalysts. Materials Advances, 2024.
23. Jing, X., et al., Enhancing Dy2O3/g-C3N4 visible photocatalytic hydrogen production performance by loading graphene-like carbon from Enteromorpha prolifera (EP-GL). Journal of Alloys and Compounds, 2024: p. 173964.
24. Sun, R., et al., Rapid charge migration of hierarchical S-Scheme g-C3N4/CdS@ C for efficient photocatalytic hydrogen evolution. International Journal of Hydrogen Energy, 2024. **55**: p. 635-644.
25. Wang, X., et al., P-N Bonds-Mediated Atomic-Level Charge-Transfer Channel Fabricated between Violet Phosphorus and Carbon Nitride Favors Charge Separation and Water Splitting. Small, 2024: p. 2311841.
26. Basyach, P., et al., Controlled Ni doping on a gC 3 N 4/CuWO 4 photocatalyst for improved hydrogen evolution. Physical Chemistry Chemical Physics, 2023. **25**(34): p. 23033-23046.
27. Chamanehpour, E., M.H. Sayadi, and M. Hajiani, Metal-organic framework coordinated with g-C3N4 and metal ions for boosting photocatalytic H2 production under sunlight. Journal of Photochemistry and Photobiology A: Chemistry, 2023. **434**: p. 114221.
28. Shi, H., et al., Hydrophilic hydrogen-bonded organic frameworks/g-C3N4 all-organic Z-scheme heterojunction for efficient visible-light photocatalytic hydrogen production and dye degradation. Journal of Photochemistry and Photobiology A: Chemistry, 2023. **435**: p. 114292.
29. Yang, T., et al., Fabrication of NiCo2S4/N-deficient g-C3N4 for efficient photocatalytic H2 production. Surfaces and Interfaces, 2023. **42**: p. 103352.
30. Tambe, A.B., et al., In situ synthesis of gC 3 N 4/Ti 3 C 2 T x nano-heterostructures for enhanced photocatalytic H 2 generation via water splitting. RSC advances, 2023. **13**(50): p. 35369-35378.